Journal of the European Ceramic Society **12** (1993) 27–41

Thermal Behavior of Polymer-derived Ceramics. I. Si–C and Si–C–O Systems from both Commercial and New Polycarbosilane (PCS) Precursors

O. Delverdier, M. Monthioux

Laboratoire Marcel Mathieu, UMR124 CNRS-DRET-UPPA, Centre Hélioparc, 2 Av. Du Président P. Angot, 64000 Pau, France

D. Mocaer & R. Pailler

Laboratoire des Composites Thermostructuraux, UMR 47 CNRS-SEP-UB1, Domaine Universitaire, 3 Allée La Boëtie, 33600 Pessac, France

(Received 14 July 1992; accepted 17 August 1992)

Abstract

Si–C- and Si–C–O-based ceramics from new or commercial polymeric precursors are compared. The emphasis is upon the structural and textural features as observed by high-resolution transmission electron microscopy (HRTEM), and their evolution with an increasing heat-treatment temperature up to 1800°C. Specifically, the behavior of an increasing excess of carbon—with regard to the Si–C stoichiometry—is revealed, and the consequences on the nucleation and the growth of the SiC grains and the electrical properties are discussed.

In dieser Arbeit werden Keramiken auf Si–C- und Si–C–O-Basis, die aus neuen oder kommerziellen polymerischen Prekursoren gewonnen wurden, miteinander verglichen. Besondere Beachtung wurde den strukturellen und den durch die Textur bedingten Eigenschaften, die mittels hochauflösender Transmissionselektronenmikroskopie (HRTEM) untersucht wurden, zugewandt. Außerdem wurde die Entwicklung dieser Materialeigenschaften mit zunehmender Temperatur bis 1800°C untersucht. Insbesondere wurde der Einfluß des Kohlenstoffüberschusses relativ zur exakten Si–C-Stöchiometrie und dessen Folgen auf die Keimbildung und das anschließende Wachstum von SiC-Körnern und auf die elektrischen Eigenschaften diskutiert.

On compare des céramiques appartenant aux systèmes Si–C ou Si–C–O et élaborées à partir de précurseurs polymériques commerciaux ou originaux. L'accent est mis sur les caractéristiques structurales et texturales révélées par microscopie électronique à transmission à haute résolution (HRTEM), et sur leur évolution au cours d'un traitement thermique croissant jusqu'à 1800°C. En particulier, le comportement d'un excès croissant de carbone par rapport à la stoechiométrie de Si–C est mis en évidence, et ses conséquences sur la nucléation puis la croissance des cristaux de SiC ainsi que sur les propriétés électriques sont discutées.

1 Introduction

Improving the physical and chemical behavior of high-performance SiC fibers requires the understanding of the thermal behavior of the polymeric precursor ceramized prior to any spinning stage (and therefore curing). Afterwards, interesting comparisons with the same but fibered then heat-treated precursor may be performed, from which the degradation mechanisms—and more specifically the role of the intrinsic oxygen from curing—may be deduced. Numerous papers have already investigated the thermal behavior of commercial SiC fibers. Rarest are papers concerned with comparative work between the uncured ceramic and the related fiber. Actually, only Yajima and coworkers[1–9] have pursued such a course of study. Rather than studying a ceramized commercial polycarbosilane (PCS) on its own, then a commercial SiC fiber (Nicalon®), it was more accurate to elaborate a laboratory ceramic fiber from this commercial PCS.

Journal of the European Ceramic Society 0955-2219/93/$6.00

The fiber obtained was chosen tentatively to be close to the commercial reference (the Nicalon® fiber) from the mechanical point of view.[10] A comparison between ceramics from the commercial PCS and from a new PCS precursor allowing higher carbon content was also made.

This paper describes the chemical, structural and microtextural aspects of the study. The ceramization and further heat-treatments are followed by TGA, elemental analysis, XRD and the investigation of electrical properties. As soon as the polymeric precursor is ceramized, i.e. the organic/mineral transition is achieved, high-resolution transmission electron microscopy (HRTEM) is the most powerful investigation technique. Indeed, because it provides textural and structural information at a nanometric scale, HRTEM is well adapted to the study of polyphasic materials such as SiC-based ceramics from polymeric precursors. The whole study inserts into a wider program, of which other results are published elsewhere[11-12] and which will act as a reference series for the study of various ceramics and laboratory fibers within the Si–C–N–O system.

2 Experimental

2.1 Samples

Two kinds of materials were prepared from a commercial PCS Mark I, after reduction of its molecular weight range (to about 1500) so that to make it able to be spun:

(i) Bulk ceramics, obtained from the pyrolysis of the PCS precursor at several temperatures.[13] These ceramics are somewhat different from those presented in Ref. 13, due to the great care taken to reduce the oxygen contamination during the procedure. This procedure allowed the fabrication of nearly oxygen-free ceramics (<2 at.%, instead of ~13 at.% without any curing step in Ref. 13) by thermolysis under argon up to 850°C (300°C/h). At this temperature the weight loss, which reached 40%, becomes negligible, and the chemical composition of the ceramized material (Table 1) is $SiC_{1.4}O_{0.05}$ (→Si–C system).

(ii) Ceramic fibers, obtained from melt spinning of the oxygen-cured PCS precursor (at 180°C)[10] then heat-treated under argon up to 850°C (300°C/h). At this temperature the weight loss, which reached 15%, becomes negligible and the chemical composition of the ceramized fiber (Table 1) is $SiC_{1.25}O_{0.54}$ (→Si–C–O system).

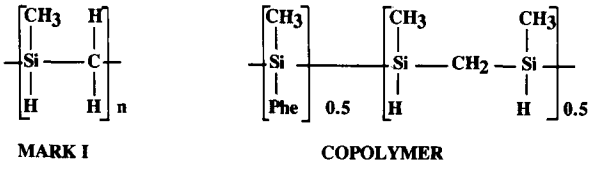

Fig. 1. Theoretical structure of the Mark I precursor,[14] and structure of the copolymer from this study.

Another ceramic material was obtained from the pyrolysis of a new PCS precursor. This PCS is a copolymer (Fig. 1) prepared[15] by adding both dichloromethylphenylsilane and bischlorosilylmethane in a molar ratio of 1 to a suspension of sodium in boiling toluene. Remaining Cl is removed with NH_3 treatment. The interest on the precursor was to obtain a ceramic material with a high carbon content in order to study the accurate role of the free carbon in the ceramic. This copolymer has a molecular weight of 1250, a softening temperature of 140–160°C. Its ceramization is considered to be achieved at 850–950°C (thermal treatment under argon), after a total weight loss of 30%. At this temperature, the chemical composition of the ceramized material (Table 1) is $SiC_{2.1}O_{0.2}$ (C-enriched Si–C system). The oxygen content originates from contamination.

The starting materials of the study are the three

Table 1. Elemental analysis (from EPMA) for both Si–C and Si–C–O (fibers) ceramics with the increasing heat treatment temperature T_p

	System								
	Si–C			*C-rich Si–C*			*Si–C–O*		
T_p °C	*Si (at.%)*	*C (at.%)*	*O (at.%)*	*Si (at.%)*	*C (at.%)*	*O (at.%)*	*Si (at.%)*	*C (at.%)*	*O (at.%)*
850	—	—	—	—	—	—	35	44	20
1000	—	—	—	30	63	7	—	—	—
1100	40	58	2	—	—	—	—	—	—
1200	41	56	2	31	62	7	36	44	19
1250	—	—	—	—	—	—	36	44	19
1400	42	57	2	31	63	6	(30)[a]	(67)[a]	2
1600	41	57	2	33	63	4	—	—	—

[a] Carbon amount is probably overestimated due to a contribution of the embedding resin.

ceramic products prepared from the procedure already described (i.e. after ceramization up to 850°C under argon). Then, a pyrolysis of these products was performed up to various end temperatures T_p from 850 to 1800°C (1 h isothermal) at 3600°C/h in graphite crucible under argon flow.

2.2 Analytical procedures

TGA analysis (SETARAM TAG 24) were performed at 600°C/h on the starting materials in a graphite crucible under purified helium flow.

Elemental analysis was performed with electron probe microanalysis (EPMA) (CAMEBAX 75) on a polished metallographic cross-section. The hydrogen contents were not able to be estimated by this technique. For the Si–C–O (fiber) system, the widespread occurrence of big crystals for the 1600°C heat treated fiber may give overestimated amounts of carbon, due to a possible contribution of the embedding resin filling up holes in the polished surface.

The electrical conductivity σ was measured from room temperature up to $\theta = 530$°C under an helium atmosphere. The measurements were performed on 10 monofilament tow sets (Si–C–O system) on alumina plates, or on fragments (Si–C system). The electrical contacts were secured with a silver lake. In the case of fragments, the shape factor is unknown. So, the comparison between fibered and bulk ceramics is mainly based on the variation of the apparent activation energy E_a with T_p (calculated from the slope of the $\log 10\sigma = f\ (1/\theta)$ graphs). However, in order to obtain conductivity values σ to the same order of magnitude for both samples, an arbitrary shape factor of 40 was taken for the fragments (Si–C system). The σ values given in Table 2 are taken at 230°C rather than at room temperature to avoid any possible machine effect for insulating materials.

2.3 HRTEM

Before HRTEM examination (Philips EM 400, 120 kV), samples were either pulverized in a boron carbide mortar (bulk ceramics) or cut by ultramicrotomy after embedding in an epoxy resin (fibers). Convenient thickness of samples for accurate HRTEM examination is less than 50 nm. The samples thus prepared are gathered on a copper grid coated with either a holey or a continuous thin film of amorphous carbon (< 10 nm).

In the electron microscope, the beam gives rise to a diffraction pattern in the image focal plane of the objective lens and to a magnified image of the specimen in the image plane. Four techniques are used to describe the material:

- —Bright field (BF): the microscope is like a light microscope of high resolving power. This mode provides informations about general texture and morphology.
- —Selected area diffraction (SAD) is used to identify the components of the material and to determine their crystallographic structure.
- —Lattice fringes (LF): an objective aperture (size: $8{\cdot}2\ nm^{-1}$) is centered on the diffraction pattern. The image is thus formed by the interference between the direct beam and a restricted number of scattered beams, giving microtextural and structural (distortions and defects) information.
- —Dark field (DF): an objective aperture is chosen small enough (size: $1{\cdot}9\ nm^{-1}$) to allow only a given *hkl* beam to go through. The part of the specimen providing the selected *hkl* beam appears bright on dark field. By displacing radially and azimuthally the objective aperture, this technique allows the exploration of the whole diffraction pattern. Successive images thus obtained give information on any preferred orientation and relative location of the various components in a polyphasic material. Figure 2 gives an example of a SAD pattern showing a powder diagram of a mixture of crystallized SiC and turbostratic carbon. β-SiC crystals are characterized by an intense 111 ring

Table 2. Changes in the electrical conductivity σ (measured at $\theta = 230$°C) and in the apparent activation energy E_a for both Si–C and Si–C–O (fibers) ceramics with the increasing heat-treatment temperature T_p; σ values are strictly comparable only within the Si–C–O system

System	T_p (°C)						
	850	*1000*	*1100*	*1200*	*1250*	*1400*	*1600*
Si–C							
$\sigma\ (\Omega\,cm)^{-1}$	10^{-9}	$1{\cdot}26 \times 10^{-5}$	—	$2{\cdot}5 \times 10^{-3}$	—	0·79	2·24
E_a (eV)	0·90	0·66	—	0·11	—	0·03	0·02
C-rich Si–C							
$\sigma\ (\Omega\,cm)^{-1}$	—	10^{-3}	0·5	—	—	2	2·25
E_a (eV)	—	0·66	0·11	—	—	0·04	0·02
Si–C–O							
$\sigma\ (\Omega\,cm)^{-1}$	3×10^{-5}	—	—	$6{\cdot}3 \times 10^{-4}$	1	1·5	—
E_a (eV)	0·66	—	—	0·33	0·05	0·01	—

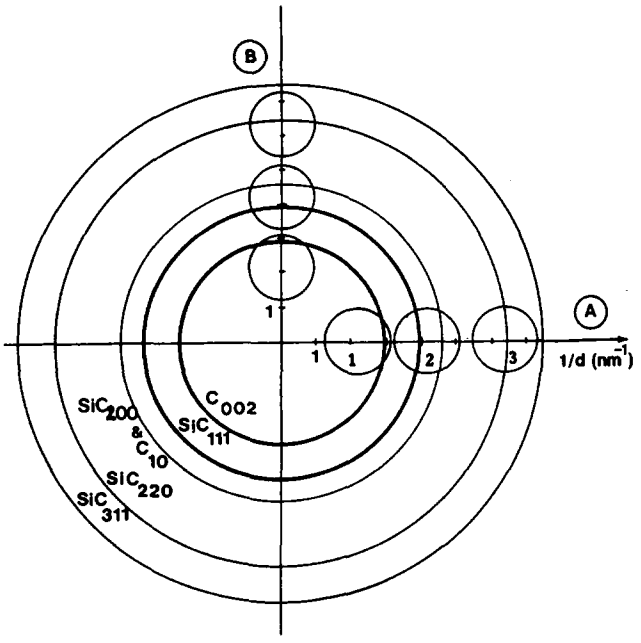

Fig. 2. Sketch of a SAD powder pattern for a material including β-SiC and turbostratic aromatic carbon. Circles represent the various positions used in the study for the objective aperture. Positions 1, 2 and 3 correspond to DF1, DF2 and DF3 dark field images, respectively.

at 3·97 nm^{-1} (0·252 nm) and two other rings 220 and 311 at 6·49 nm^{-1} (0·154 nm) and 7·63 nm^{-1} (0·131 nm). The 200 ring at 4·59 nm^{-1} (0·218 nm) is generally not visible on a normally exposed SAD pattern. Turbostratic carbon is characterized by a 002 ring at about 2·9 nm^{-1} (0·344 nm or more) and two joint and asymmetrical bands 10 and 11 at 4·8 nm^{-1} (0·21 nm) and 8·3 nm^{-1} (0·12 nm). On this pattern are superimposed the various positions used in this study for the objective aperture location. The 0·9 nm^{-1} aperture size allows a resolution of 0·65 nm. The positions 1, 2 and 3 respectively are centered on 2·1, 4·3 and 6·2 nm^{-1}, permitting the azimuthal twist tolerances ±27°, ±13° and ±9°. Likewise, the aperture admits respectively scattered beams corresponding to interplanar distance ranges of 0·32 to 0·9 nm (position 1 = DF1), 0·19 to 0·3 nm (position 2 = DF2) and 0·14 to 0·19 nm (position 3 = DF3). If amorphous SiO_2 is present, its most intense halo (at 0·44 nm) is taken together with C_{002} in position 1 of the aperture. Thus, confusion could be possible. However, dark field and bright field features (porosity, diffusion contrast, etc.), allow C or amorphous silica to be determined. Likewise, the contribution of the C_{10} signal is weak compared to the SiC_{111} signal and can be neglected in the DF2 images. Eventually the position 3 allows images of SiC alone to be obtained. The positions B are rotated through an angle of 90° relative to positions A, illustrating the azimuthal exploration of the reciprocal space, which is able to provide textural information (preferred orientations of crystallized phases for example).

3 Results

3.1 Physicochemical

The weight losses for the ceramized fibers (Si–C–O system) and the bulk ceramics (Si–C system) are reported in Fig. 3. The weight loss of ceramic fibers is very low up to 1250°C. Then it reaches 25% at 1500°C and remains stable above this temperature. The weight loss for the Si–C system is very low and slow, and reaches only about 4% at 1500°C. This thermal stability is sustained by the chemical composition, which remains unchanged up to 1600°C at least, both for the Si–C system and the C-enriched Si–C system (Table 1). In contrast, the chemical composition of fibers (Si–C–O system) is stable up to 1250°C only. At 1400°C, the fiber composition is dramatically modified, and exhibits a strong decrease in the oxygen content. Silicon content also seems to decrease strongly, with a subsequent increase in carbon content. This latter effect goes against previous statements obtained for the Nicalon® fiber,[16,17] and moreover is not supported by the TEM observations (see Section 3.2.3). Therefore, the enrichment in carbon is assumed to be due to a contribution of the embedding resin, which may fill the porosity created by the weight loss and/or the voids left by SiC crystals which have pulled out.

3.2 Structural and textural (HRTEM)

3.2.1 Si–C system

3.2.1.1 BF images and SAD pattern. The BF images of Fig. 4 illustrate the textural evolution of the bulk ceramic with the increasing heat-treatment from 900 to 1800°C. At the lowest temperature (900°C) a fine granular texture appears (Fig. 4(a)) which is attributed to a fine porosity rather than to numerous small crystals, since the material is found to be amorphous. Indeed, the related SAD pattern (in insert) shows two diffuse haloes located at about 3·98 and 6·57 nm^{-1} corresponding respectively to 0·25 and 0·15 nm, which characterize an amorphous SiC-based material. The pore size is around 1 nm.

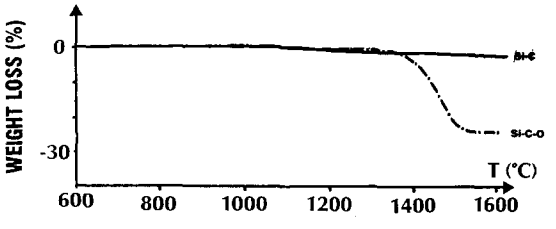

Fig. 3. Weight losses recorded from TGA for the Si–C system (———) and the Si–C–O system (– · – · –).

When heat-treated at higher temperatures (Fig. 4(b) to (d)), the texture remains granular but a global aspect evolves progressively. The related SAD patterns indicate that the material is crystallized from 1100°C, since all the reflections of β-SiC are found: 0·252 nm (111), 0·154 nm (220) and 0·131 nm (311) among others. Thus, the granular aspect is now mainly due to the presence of numerous SiC crystals, the size of which increases with the increasing temperature. The increasing size of crystals is obvious at 1400–1600°C and 1800°C on the BF images (Fig. 4(c) and (d)), and can be followed from 1100°C by the width of the diffraction rings on the SAD patterns, which become sharper and sharper and spotted with the increasing temperature. Crystal sizes are easily measured from the BF

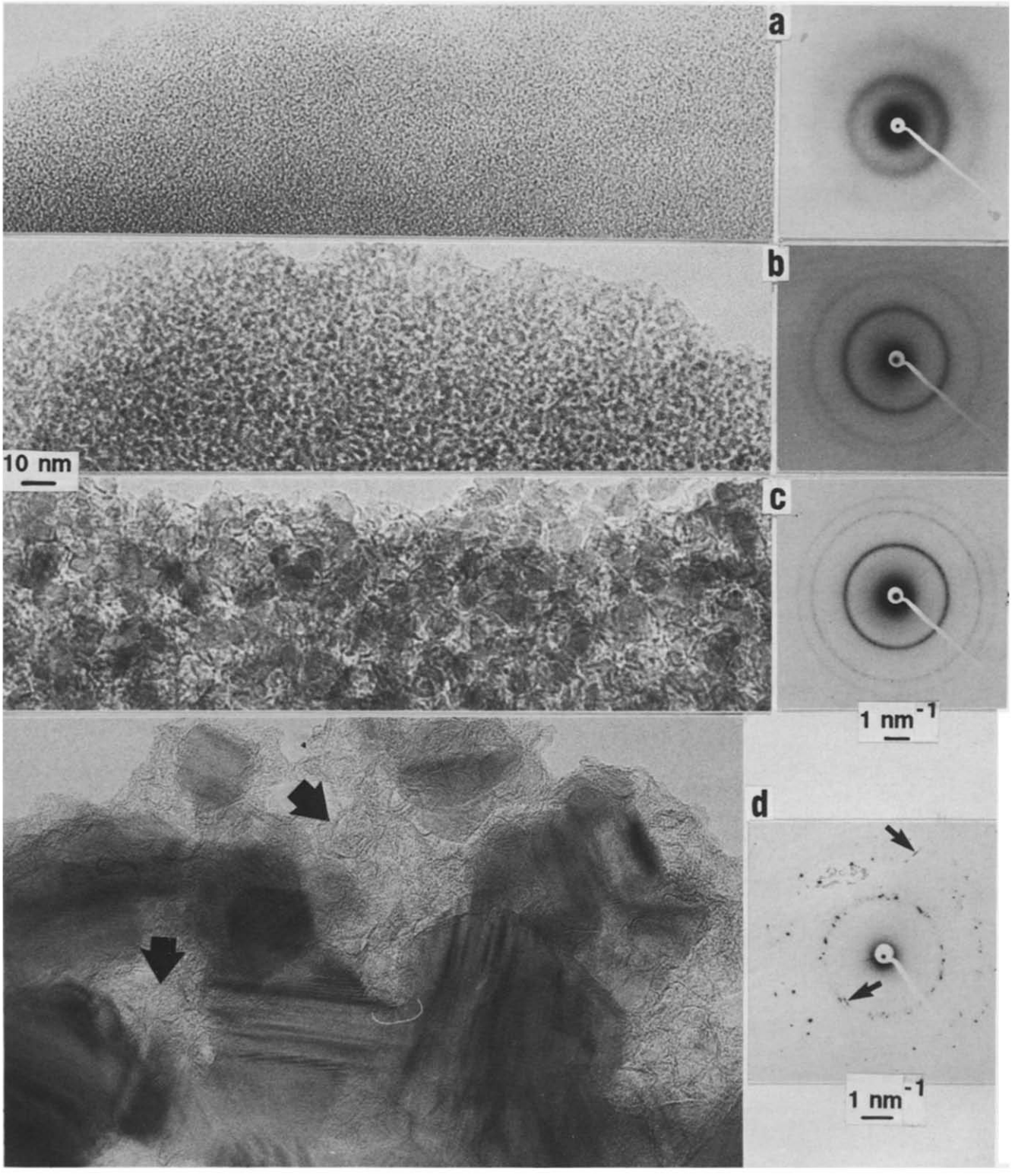

Fig. 4. Bright field images of the ceramics from the Si–C system with increasing T_p. (a) 900°C, (b) 1000–1200°C, (c) 1400–1600°C, (d) 1800°C. The related diffraction electron patterns are inserted.

images at 1800°C (Fig. 4(d)), but are hardly in evidence for the lower temperatures. Such measurements will then be performed from the DF images (see Section 3.2.1.2). Anyway, SiC crystals are always β-SiC, but some polytypism appears at the highest temperature (1800°C), as shown on the related SAD pattern (arrows).

Besides the SiC phase, the material also contains free carbon. At 1800°C, the free carbon appears obvious in BF images. It forms a porous phase located between the SiC crystals (arrows in Fig. 4(d)). The DF and LF images (see Sections 3.2.1.2 and 3.2.1.3) show that some free carbon is present at least from 1000°C.

3.2.1.2 Dark-field images. Figure 5 illustrates the DF1 images (see Section 2) corresponding to Fig. 4. At 900°C (Fig. 5(a)) the image shows bright dots, the size of which is that of the resolution limit δ determined by the opening of the objective aperture used ($\delta = 0{\cdot}65$ nm for the $1{\cdot}9\ \text{nm}^{-1}$ aperture) following the relation:

$$\delta = 0{\cdot}61\lambda/\alpha$$

where λ is the wavelength and α the half-opening angle of the objective lens (which is limited by the objective aperture).

When successive DF1 images are taken together with increasingly defocusing the objective lens, the bright dots quickly disappear, while others appear. All the dots seem well focused whatever the focus value Δf_0 (Fig. 6). Consequently, the dots are dimensionless and do not represent real objects. Therefore, it is ascertained that no periodic structure of aromatic free carbon are present, even as primary entities such as BSUs (basic structural units). BSUs are face-to-face associations of two to three aromatic carbon layers (diameter < 1 nm) stacked in turbostratic order.[18] They are commonly encountered in most carbon materials near the end of primary carbonization.[19]

Figure 5(b) shows a DF1 image illustrating the 1000°C heat-treated sample. Dots are fewer. The size of dots is bigger (1–2 nm) than the resolution limit, thus they are real objects. Because of the lack of oxygen within the material composition, silica is excluded. Therefore, each dot is a small stack of

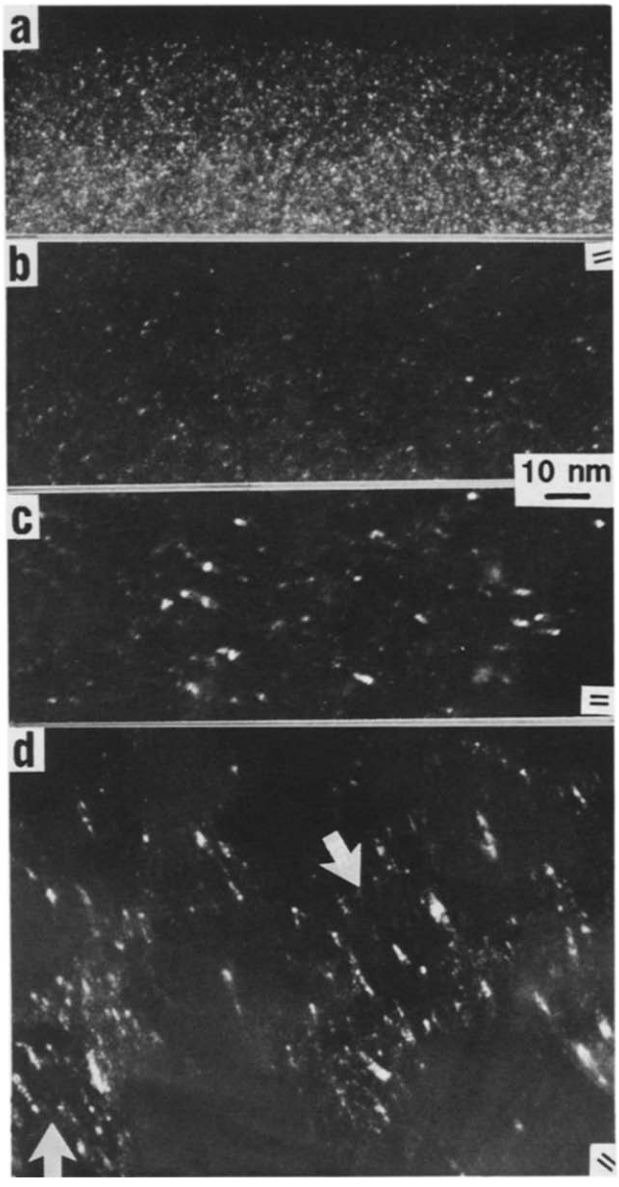

Fig. 5. Position 1 dark field images of the ceramics from the Si–C system with increasing T_p. (a) 900°C, (b) 1000–1200°C, (c) 1400–1600°C, (d) 1800°C.

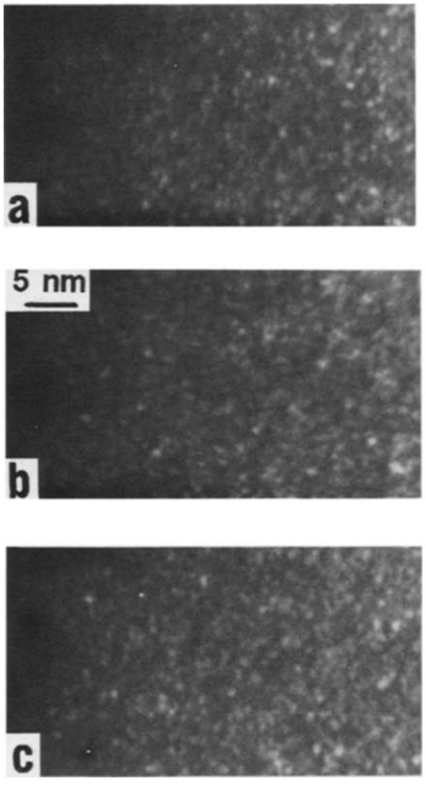

Fig. 6. Position 1 dark field images with an increasing defocusing of the objective lens for an amorphous material from the Si–C system ($T_p = 900$°C). (a) $\Delta f_0 = 0$, (b) $\Delta f_0 = 160$ nm, (c) $\Delta f_0 = -320$ nm.

planar aromatic structures piled up following their *c* axis and presenting the (00·1) planes parallel to the electron beam. The thermodynamic state of the material excludes a structural order other than turbostratic. With increasing T_p (Fig. 5(c) to (d)), the shape of the dots becomes elongated and may reach 8–9 nm at 1800°C. The direction of aromatic layers (double bars in Fig. 5(b) to (d)) is always parallel to the elongation axis of the dots, indicating that the primary aromatic carbon stacks tend to link edge-to-edge with increasing T_p. Again, this is a common behavior in most carbon material.[19] Up to 1600°C orthogonal DF1 images give similar aspects with the free carbon located randomly between SiC crystals (see Section 3.2.1.3). Consistent with previous studies, the aromatic free carbon thus tends to form a network of open cages around SiC crystals.[20] In contrast, at 1800°C, areas free of any SiC grains and made of free carbon only are found in the material (Figs 4(d) and 5(d), arrow).

Figure 7 illustrates the evolution of the DF2 images with the increasing T_p. Figure 7(a) ($T_p = 900$°C) shows the very small bright dots which characterize the amorphous state, as already described for the DF1 images.

In Fig. 7(b) ($T_p = 1000$, 1100 and 1200°C) and Fig. 7(c) ($T_p = 1400$ and 1600°C) some of the SiC crystals contained in the material are lit up as soon as their (111) lattice planes are under the Bragg angle. Other SiC crystals are lit up—and similar images are obtained—when the objective aperture is located at other positions around the 111 diffraction ring. Such images are used to determine the modal (i.e. the most frequent) and the maximal sizes of SiC grains. At 1000°C (not illustrated) the modal crystal size is 2 nm, with a maximal size at 4–5 nm. At 1100 and 1200°C (Fig. 7(b)) the modal crystal size is about 2–3 nm and 3 nm, respectively, with a maximal size at 5 nm. At 1400 and 1600°C (Fig. 7(c)) the modal size is 8–10 nm and 10 nm, respectively, with maximal sizes around 20 nm. At 1800°C (Fig. 7(d)), due to the Bragg conditions which are more drastic for big crystals, both BF and DF images have to be used to determine the crystal sizes. Compared to the lower temperatures, the histogram of crystal size is much wider, from less than 15 nm up to 100 nm (Fig. 8). Such a change in histogram shape indicates a change in the mechanism of grain growth towards a coalescence by impingement at 1800°C.[17,21] Some crystals (arrow on Fig. 7(d)) exhibit stacking faults, which reveals a rapid growth.

3.2.1.3 LF images. For the 1000°C heat-treated sample (Fig. 9(a)), the free carbon is observed as small stacks of two to three distorted layers with length $\leqslant 2$ nm. The distance between two fringes is at least 0·344 nm, which is the minimal interplanar

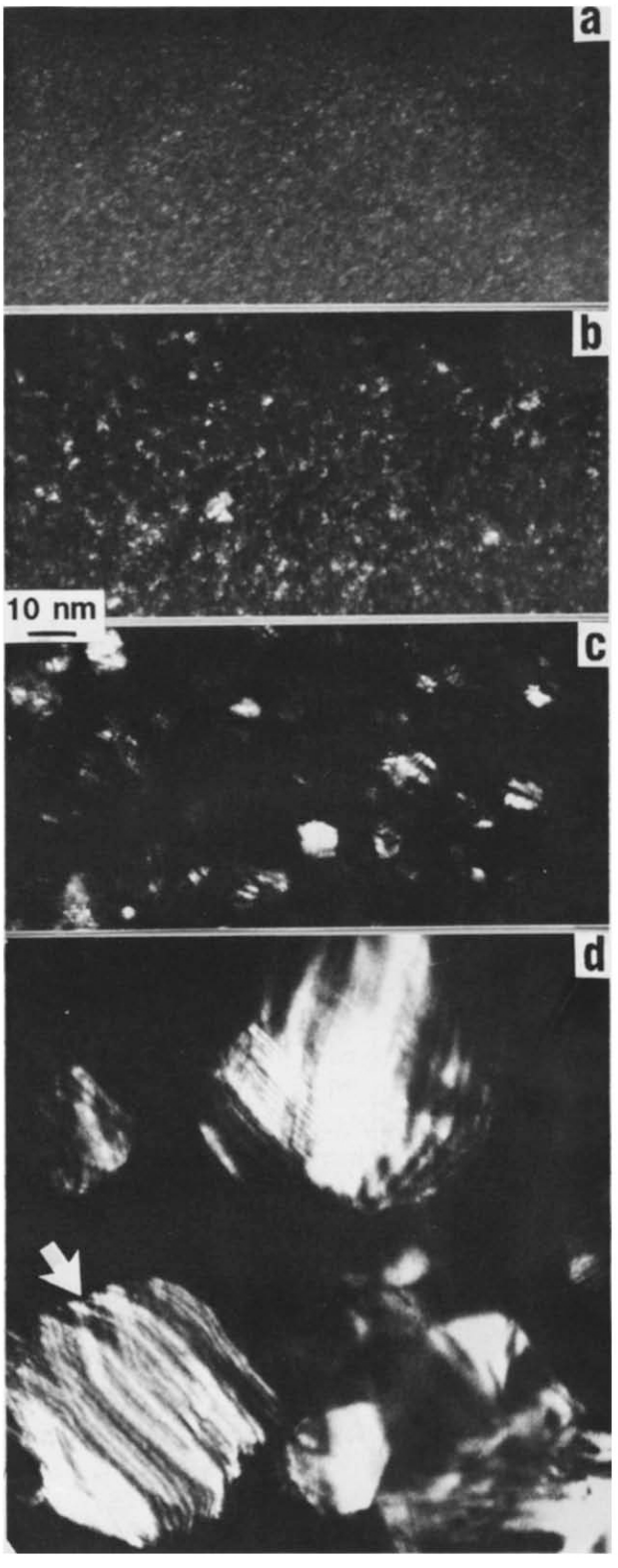

Fig. 7. Position 2 dark field images of the ceramics from the Si–C system with increasing T_p. (a) 900°C, (b) 1000–1200°C, (c) 1400–1600°C, (d) 1800°C.

value for turbostratic carbon.[22] SiC crystals are revealed by their (111) SiC lattice fringes, which are always very sharp, straight and parallel (arrow). The distance between two fringes is 0·25 nm. With increasing T_p, the number of carbon layers within a carbon stack does not change markedly (always around 2–6 layers). In contrast, the length of carbon

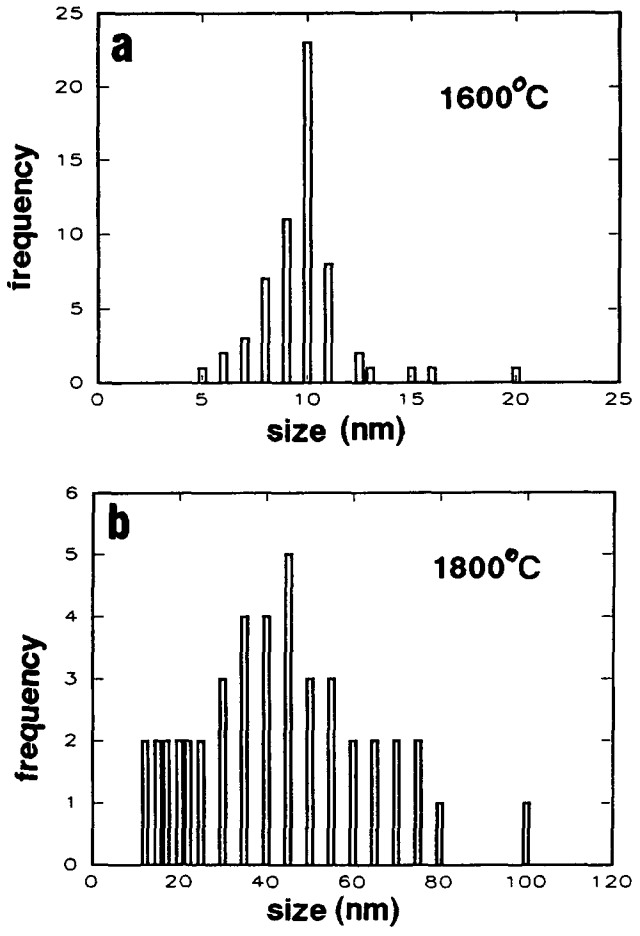

Fig. 8. Histograms of SiC crystal size of ceramics from the Si–C system. (a) 1600°C, (b) 1800°C.

layers increase due to edge-to-edge linkages: 3–4 nm at 1100–1200°C (Fig. 9(b)), 5–6 nm at 1400–1600°C (Fig. 10) and up to 10–12 nm at 1800°C (Fig. 11(b)). In the same way, the increasing temperature makes the structural organization of the carbon stacks improve, due to the removal of some structural defects (i.e. the stiffness of the layers improves). As a consequence of the crystal growth, which makes the available grain boundary area decrease, the relative amount of free carbon apparently seems to increase. Similarly to what is observed in heat-treated ceramics from the same system[20] or from a different system (Si–C–N),[12] carbon stacks tend to lie flat upon the SiC crystal faces (arrows in Fig. 10, for example), suggesting the occurrence of incomplete carbon cages around crystals.

At 1800°C, besides the drastic growth of crystals (Fig. 11(a)) the free carbon is found either still associated flat upon the SiC crystals (Fig. 11(a)) or located randomly between them as a porous phase, the pores being free of any crystal (Figs 4(d) and 11(b)). Obviously, the SiC crystals leave the carbon cages for $T_p > 1600$°C, due to the fact that the respective sizes of carbon cages and crystals are no longer compatible.

3.2.2 C-Enriched Si–C system

The global changes in textural features with increasing T_p are similar to that of the Si–C-based ceramics studied above. However, at 1000°C, the material is still amorphous regarding the SiC phase (Fig. 12(a)) while the crystallization of β-SiC has already occurred in the previous Si–C system at this temperature (Fig. 4(b)). Correspondingly to the higher carbon content (C/Si atomic ratio = 2·1 instead of 1·4, see Table 1), the free carbon is now abundant enough to give rise to an observable pattern in the SAD images from 1000°C (Fig. 12(a)) and higher heat-treatment temperatures (Fig. 12(b) and (c)). At 1000°C, the LF images (Fig. 13(a)) show that the free carbon structure is BSU (arrows) indicating that the aromatic carbon layers are at the primary step of organization. At 1200°C, the crystallization of SiC has occurred (Fig. 12(b)). With increasing T_p, the crystal size increases but in to a lower extent than for the previous Si–C system: at 1200°C the modal size is 2 nm with a maximal size at 4 nm, at 1400°C the modal size is 5 nm with a maximal size at 10 nm, and at 1600°C the modal size is 7 nm with a maximal size at 15 nm. Similarly, the structural organization of the distorted carbon layers also improves, but always remains lower than for the previous system, since the mean layer length is < 1 nm at 1000°C and reaches ~4 nm at 1600°C (Fig. 13(b)), while it is 1–2 nm and 5–6 nm respectively for the same temperatures in the previous Si–C

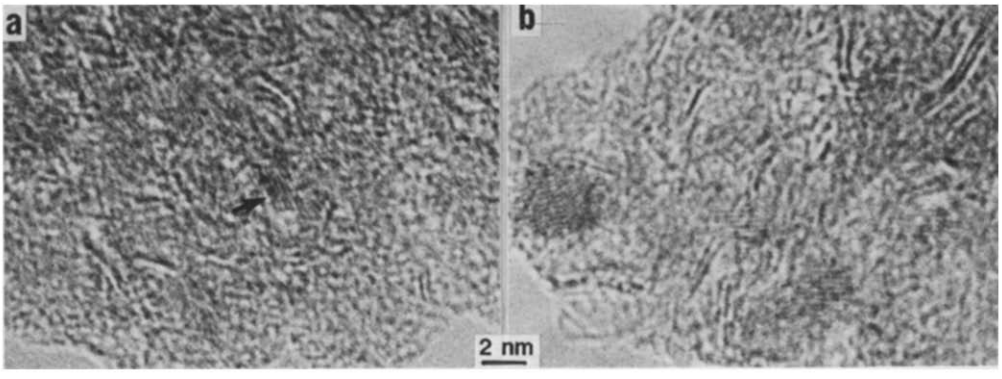

Fig. 9. Lattice fringe images of ceramics from the Si–C system. (a) T_p = 1000°C, (b) T_p = 1100–1200°C.

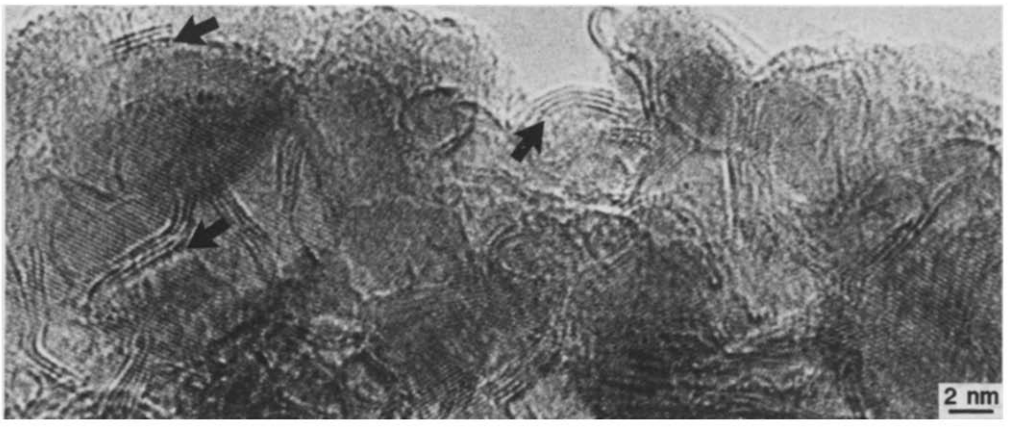

Fig. 10. Lattice fringe images of a ceramic from the Si–C system. $T_p = 1400$–$1600°C$.

system. Anyway, the behavior of carbon is identical to the previous statement, i.e. arranged in open cages around the SiC grains (Fig. 13(b)).

3.2.3 Si–C–O system (fibers)

Up to $T_p = 1200°C$ the fibers exhibit a nanometric porosity such as in Fig. 4a.[10] Both the SAD pattern[10] and the focus series in dark field such as in Fig. 6 characterize an amorphous state. However, DF1 images indicate that the fibers are coated with a turbostratic carbon film (thickness ~ 5 nm), in which the aromatic planes are somewhat parallel to the fiber surface.[10] This carbon film is observable up to $T_p = 1400°C$. An example is given for $T_p = 1350°C$ (see Fig. 16(a)). Because this carbon film appears before the occurrence of free carbon within the fiber, it is assumed to originate from the thermal cracking of residual hydrocarbon species coming from the fiber.

For $T_p = 1250°C$, the textural aspect does not change but the DF1 focus series images indicate the occurrence of free carbon as BSUs. Indeed, despite the defocusing of 320 nm, some bright dots remain observable, although their size is close to the resolution limit $\delta = 0{\cdot}65$ nm (Fig. 14, arrows). Therefore, they are real objects. In contrast, SiC is not yet crystallized.

For $T_p = 1350°C$, a skin/core effect occurs, marked by a textural change. The skin thickness is $\sim 3\ \mu m$. Within the fiber core, β-SiC crystals are now widely present, with a modal size at 1–2 nm and a maximal size at 4 nm (Fig. 15(b)). Free carbon is also obvious as small bright dots in DF1 images (Fig. 15(a)) or as small aromatic layer stacks (length ~ 2 nm) in LF images (Fig. 17(b)). In contrast, carbon stacks are no longer visible around crystals in the fiber skin, either in DF1 images (Fig. 16(a)) or in LF images (Fig. 17(a)). This is obvious from the

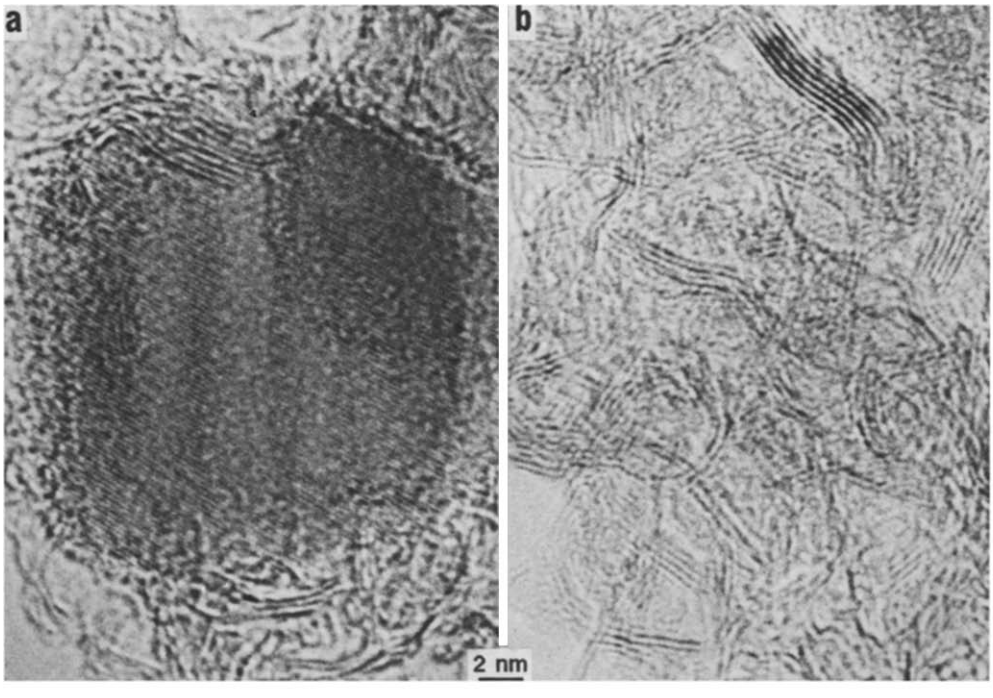

Fig. 11. Lattice fringe images of the ceramic from the Si–C system. $T_p = 1800°C$. (a) Zone with both C and SiC phases, (b) zone free of SiC crystals.

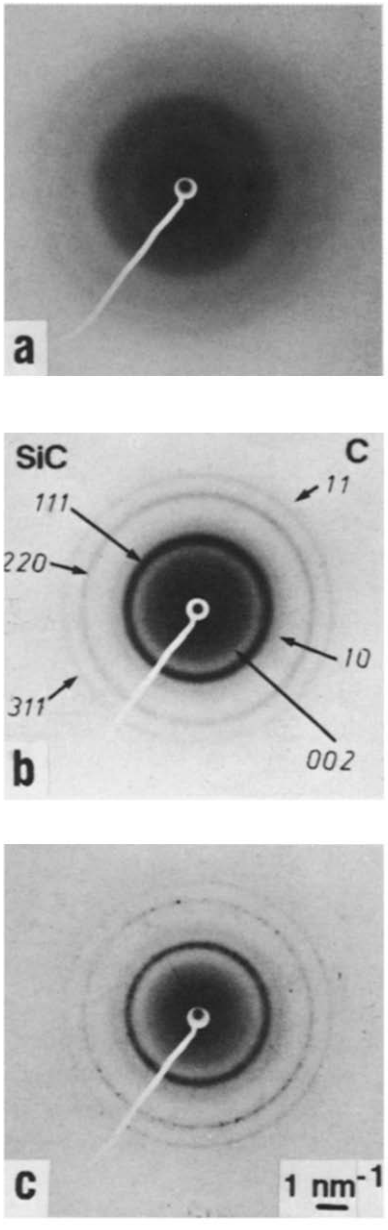

Fig. 12. SAD patterns for ceramics of the C-enriched Si–C system. (a) $T_p = 1000°C$, (b) $T_p = 1200°C$, (c) $T_p = 1600°C$.

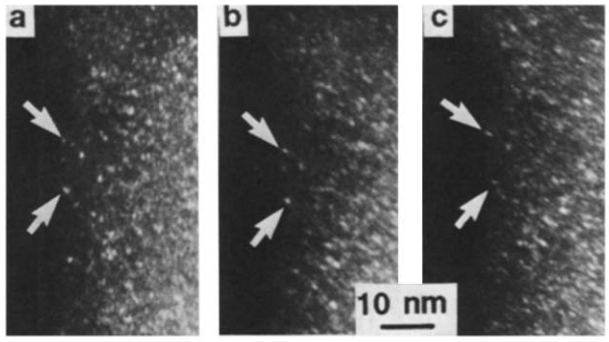

Fig. 14. Position 1 dark field images with an increasing defocusing of the objective lens for a ceramic fiber from the Si–C–O system. $T_p = 1250°C$. (a) $\Delta f_0 = 0$, (b) $\Delta f_0 = -160$ nm, (c) $\Delta f_0 = -320$ nm. Arrows indicate BSUs.

comparison between Fig. 16(a) and the DF1 images of the core (Fig. 15(a)) or the DF1 images of a 1400°C heat-treated ceramic from the Si–C system (Fig. 5(d)), in which crystal sizes are similar. Compared to the fiber core (Fig. 15(b)) the SiC grains have grown drastically (Fig. 16(b)), with a modal size which is changing from the outer part to the inner part within the fiber skin, following a decreasing gradient from 7 to 4 nm. Obviously, this skin/core effect is reminiscent of the identical effect observed in a Nicalon® fiber.[16,21,23] Therefore, the degradation mechanisms of both Si–C–O fibers are identical and should follow the path described elsewhere:[17] release of gaseous SiO from Si–O–Si and Si–O–C bonds[8] (which were located in a SiO_xC_y intergranular phase[17,24]), endogeneous oxidation of the free carbon network by SiO and subsequent release of CO, subsequent drastic growth of SiC grains according to a coalescence mechanism, allowed by the concomitant alteration of both the SiO_xC_y and free carbon intergranular phases.

For $T_p = 1400°C$ the structural and textural features of the skin at $T_p = 1350°C$ have invaded the whole fiber,[10] indicating that the fiber degradation has proceeded and is controlled by the diffusion of the gaseous species. However, a continuous coating

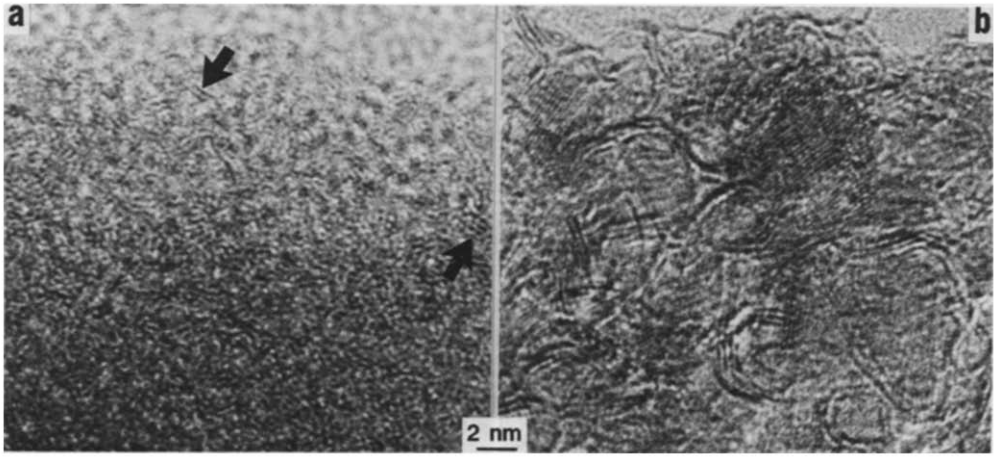

Fig. 13. Lattice fringes images of ceramics from the C-enriched Si–C system. (a) $T_p = 1000°C$, (b) $T_p = 1600°C$.

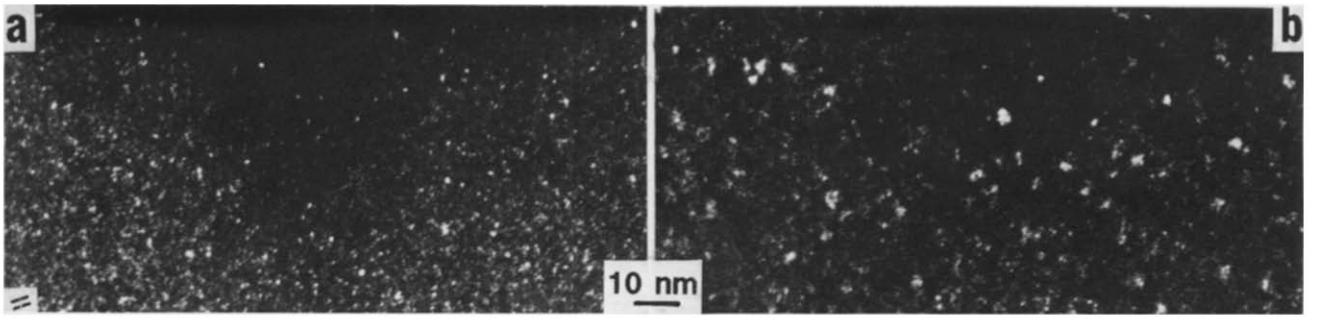

Fig. 15. Dark field images of the inner part of a ceramic fiber from the Si–C–O system. $T_p = 1350°C$. (a) DFI: bright dots are carbon stacks; only stacks with aromatic layers parallel to the double bars are imaged, (b) DF2: bright dots are SiC crystals.

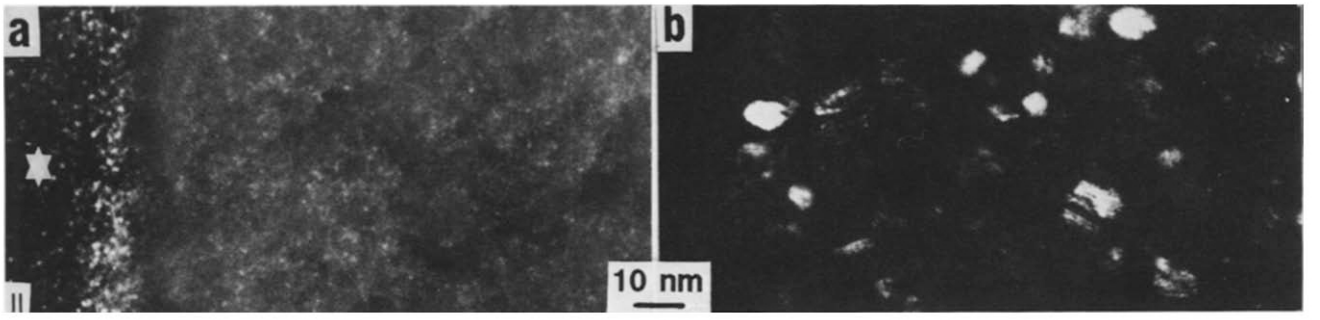

Fig. 16. Dark field images of the outer part of a ceramic fiber from the Si–C–O system. $T_p = 1350°C$. The star indicates the embedding resin. (a) DF1: the free carbon has degraded. The bright rim at the fiber surface reveals an outer carbon film made of turbostratic carbon (undegraded) statistically oriented parallel to the double bars. (b) DF2: the SiC crystals have drastically grown.

of a microporous aromatic carbon is observed at the fiber surface (thickness ~ 40 nm),[10] in addition to the oriented carbon film already observed from $T_p = 1100°C$. Surprisingly, this microporous carbon coating was not yet observed for $T_p = 1350°C$ and is no longer observed for $T_p = 1600°C$. This indicates that the occurrence and the disappearance of outer free carbon cannot be related to the endogeneous oxidation event. In addition, such aromatic carbon cannot originate from the mere SiC decomposition within the experimental conditions used, since vacuum is required below the normal decomposition temperature.[25,26] Therefore, it is assumed that this carbon coating could originate from the oxygen impurities in the argon atmosphere, through the thermodynamically favorable reactions of a low partial pressure of CO on SiC.

$$SiC(s) + CO(g) \rightarrow SiO(g) + 2C(s)$$

or maybe[27]

$$2CO(g) \rightarrow CO_2(g) + C(s)$$

CO possibly being formed from the oxidation of environmental carbon (crucible, furnace walls). The need for specific thermodynamic conditions (temperatures, partial pressures of SiO and CO) could account for the exclusive occurrence of the carbon coating for the single heat-treatment temperature $T_p = 1400°C$.

For $T_p = 1600°C$, the drastic crystal growth has

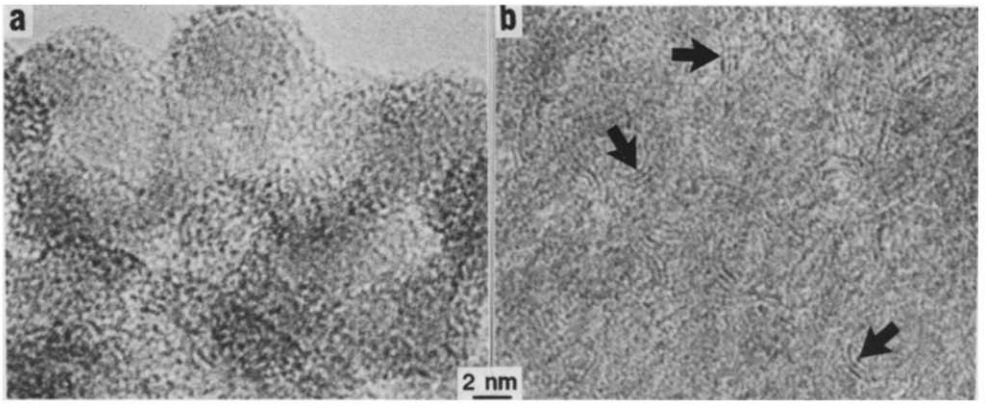

Fig. 17. Lattice fringes images of a ceramic fiber from the Si–C–O system. $T_p = 1350°C$. (a) Outer part (skin): carbon stacks are no longer visible. (b) Inner part (core): carbon stacks are arrowed.

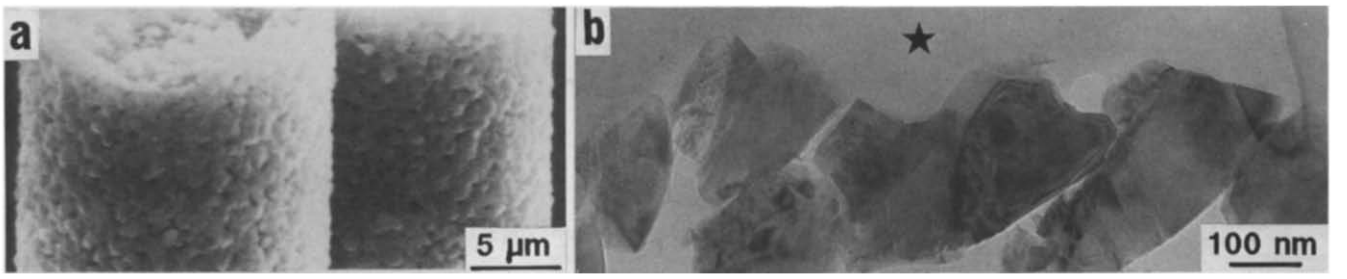

Fig. 18. Ceramic fiber from the Si–C–O system. $T_p = 1600°C$. (a) SEM image; (b) bright field image of the outer part of the fiber. The star indicates the embedding resin.

still proceeded so that the modal crystal size becomes difficult to estimate. From both SEM (Fig. 18(a)) or TEM images (Fig. 18(b)), grain sizes range from 20 nm to about 1 μm. The total disappearance of carbon is obvious either at the fiber surface or within the fiber.

4 Discussion

4.1 Thermal behavior of the free carbon

As a common behavior in any carbon material,[18,19] BSUs are the primary periodic aromatic entities to appear with an increasing heat-treatment. Each BSU is isolated and the peripheral carbon atoms are saturated by hydrogen atoms. Such aromatic CH groups are not stable at high temperature, and hydrogen is removed as H_2 in the 1000–1200°C range. This induces unsaturations which are eliminated by the edge-to-edge linkage of neighboring BSUs into larger distorted stacks.[19] This common behavior seems also true for many carbon-containing ceramic materials:[11,12,17,20,28,29] BSUs appear, always before the first SiC crystals, then link edge-to-edge into incomplete carbon cages around the SiC grains, which may give rise to a genuine interconnected carbon network afterwards.[20] Both the BSU stage and carbon-cage stage are able to be revealed by HRTEM. In contrast, HRTEM cannot say whether carbon cages are interconnected at long distance or not. This will be revealed by the change in electrical properties[20] (see Section 4.4).

Surprisingly, the BSU stage is not found within the Si–C system (atomic ratio C/Si = 1·4), and free carbon is directly observable as distorted stacks from $T_p = 1000°C$. This could suggest either that both the appearance of BSUs and the hydrogen release occur between $T_p = 900$ and 1000°C, or that the initial hydrogen content of the material was not enough to allow isolated BSUs to be maintained (atomic ratio H/C for BSUs is ~0·5[20]). The latter hypothesis would induce a quasi-concomitant primary connection between neighboring BSUs (by 2 or 3) into small distorted stacks, in order to reach the convenient H/C value (atomic ratio H/C < 0·5). It is noteworthy that, in contrast, the BSU stage is observed both in the C-enriched Si–C system (atomic ratio C/Si = 2·1) and the Si–C–O system.

4.2 Thermal evolution of the ceramics within the Si–C system

4.2.1 Si–C system (atomic ratio C/Si = 1·4)

The bulk thermal behavior may be summarized as follows:

Stage 1 (900–1000°C). The vitreous–crystallized transition occurs, both for the SiC phase (β) and the free carbon (bidimensional crystals). Boundaries between SiC cannot be otherwise than Si–C tetrahedra and aromatic free carbon. The free carbon progressively arranged into incomplete cages around crystals.

Stage 2 (1000–1400°C). A primary coarsening of SiC grains occurs, then accelerates with the increasing temperature. It is probably due to the rearrangement of atoms at the grain boundaries rather than to a 'feeding' from an amorphous SiC phase (which has not been detected at this stage). The textural and structural organization of the carbon network improves.

Stage 3 (1400–1600°C). The primary crystal growth is momentarily inhibited (Fig. 19), which may be due to the exhausting of the possibilities of grain boundary rearrangements, but probably mainly due to a hindering by the carbon network.

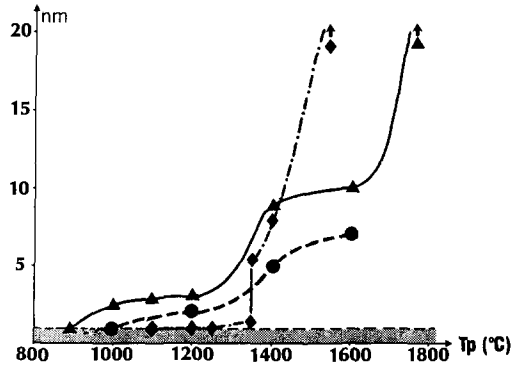

Fig. 19. Modal sizes of SiC crystals versus increasing T_p for the ceramics from (▲) Si–C, (●) C-enriched Si–C, and (◆) Si–C–O systems.

Indeed, starting from a given volume of free carbon, the crystal growth makes the total crystalline surfaces decrease and therefore makes the amount of free carbon at the crystal boundaries increase relatively.

Stage 4 (> 1600°C). A rapid secondary crystal growth occurs (Fig. 19). It is due to the fact that the SiC crystals are expelled from the carbon network, and therefore become free to coalesce by impingements. This is favored by the high temperatures T_p. The expulsion may be promoted by internal stresses induced by the continuous structural and textural improving of the carbon network. Structural change $\beta \rightarrow \alpha$ or polytypes for SiC crystals occurs at least from 1800°C.

The bulk chemical composition of the system does not change and remains in excess of carbon with regard to the stoichiometry of SiC.

4.2.2 The role of excess free carbon

The comparison between the Si–C system (atomic ratio C/Si = 1·4) and the C-enriched Si–C system (atomic ratio C/Si = 2·1) shows that:

(i) An excess of free carbon delays the occurrence of the first SiC crystals (for 100–200°C higher T_p).
(ii) An excess of free carbon inhibits the primary crystal growth (Fig. 19).

The reason why high amounts of carbon within the material also delay the occurrence of the first BSUs is not understood yet.

4.3 Si–C–O system (fiber)

4.3.1 Summary of the bulk thermal behavior

Stage 1 (< 1250°C). The material is amorphous.
Stage 2 (1250–1350°C). Free carbon appears as BSUs within the amorphous phase. β-SiC crystals appear afterwards. Carbon BSUs arrange into incomplete carbon cages around SiC grains. Oxygen is included as Si–O–Si or Si–O–C groups[8] in another intergranular phase, made of a continuum of SiO_xC_y tetrahedra, according to the model already proposed for the Nicalon® fiber.[24]
Stage 3 (≥ 1350°C). As in a Nicalon® fiber,[16,17,21] the oxygenated groups degrade, providing mainly gaseous SiO. SiO may in turn oxidize the free carbon, providing CO. The sudden degradation of both intergranular phases (SiO_xC_y continuum and carbon network) leaves the SiC grains free to coalesce by impingements inducing a rapid growth. Because reactions are governed by gas diffusion, the phenomenon proceeds from the surface to the core inducing both a skin/core effect and a gradient of crystal sizes within the skin.

The bulk chemical composition of the system tends towards the stoichiometry of SiC.

4.3.2 The role of intrinsic oxygen

Since the atomic ratios C/Si are similar (atomic ratio C/Si = 1·3–1·4), the comparison between ceramics for both Si–C and Si–C–O systems provides accurate information on the role of intrinsic oxygen. Below the degradation temperature of the SiO_xC_y phase (~ 1300°C), oxygen is beneficial:

(i) Oxygen delays by ~ 200°C the occurrence of both the first SiC crystals and BSUs.
(ii) Oxygen delays the primary crystal growth, due to the widespread presence of the SiO_xC_y intergranular phase, hindering structural rearrangements at the grain boundaries.

Above the degradation temperature of the SiO_xC_y phase, the effect of oxygen is catastrophic:

(i) Endogeneous oxidation of the carbon network and subsequent high weight loss (SiO, CO).
(ii) Early drastic secondary crystal growth, induced by the early ability of SiC grains to coalesce freely.

4.4 Relationships with electrical properties

Table 2 provides the σ and E_a data for both systems. It is recalled that, due to the shape factors which are not known for the non-fibered ceramics, σ values are only indicative and may be used for comparisons only within the Si–C–O system.

Figure 20 indicates the changes of E_a with increasing T_p. The strongest decrease in the E_a value for the Si–C system (atomic ratio C/Si = 1·4), i.e. the fastest improvement of the conductive feature of the material, occurs in the 1000–1200°C range. Obviously, no structural event but the completion of the carbon network can be related to this decrease of E_a: the SiC crystal growth is almost nil and the chemical

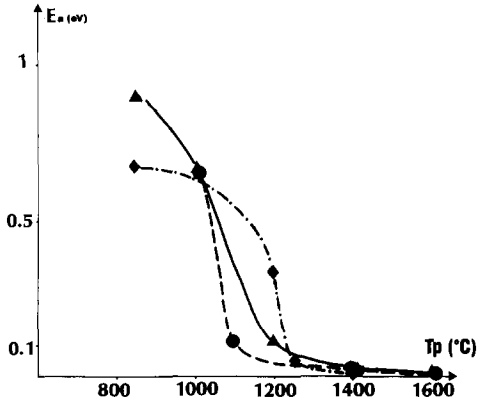

Fig. 20. Apparent activation energy E_a for conductivity versus increasing T_p for the ceramics from (▲) Si–C, (●) C-enriched Si–C, and (◆) Si–C–O systems.

composition remains stable, at least regarding the Si and C content (Table 1). In contrast, the decrease in E_a occurs in the same temperature range as the hydrogen release in carbon materials.[19]

According to previous studies,[20] this drop in E_a value is thus related to the progressive but rapid interconnection of the carbon stacks within the material. Identically, the decrease in E_a starts at the same T_p for the C-enriched Si–C system, but falls more quickly (Fig. 20). This may be related to an earlier interconnection of the carbon network, which is logically related to an expected higher initial amount of free carbon.

Similarly, the strongest decrease in E_a for the Si–C–O system cannot be related to any structural or textural event but rather to the behavior of free carbon: SiC crystals have not yet appeared in the 1200–1250°C temperature range, and the chemical composition remains stable, at least regarding the Si, C, O content (Table 1). In contrast, this temperature range corresponds to the very moment of the occurrence of free carbon as BSUs. Nevertheless, it is surprising that isolated BSUs are able to make the conductivity increase so quickly (almost four decades). This could be related to the peculiar feature of these BSUs, which are formed too late (regarding the temperature of hydrogen removal) to be saturated with peripheral hydrogen atoms as in other Si–C[20] or Si–C–N[11,12] systems. Finally, even though the carbon network is destroyed, the conductivity of the fiber is maintained at high temperature ($T_p > 1400$°C). Actually, as already mentioned for the Nicalon® fiber,[17] the conductivity, after being controlled by the behavior of the free carbon, is then controlled by the widely crystallized SiC phase.

5 Conclusion

From the data above, it is obvious that oxygen is not desirable, and neither is another heteroatom such as nitrogen.[12] The simpler is the system, the more stable it is. This statement is supported by actual efforts to tentatively develop oxygen-free curing processes for ceramic fibers. Contrarily to a widespread opinion, excess free carbon does not necessarily have to be avoided, since it is beneficial to the material by hindering the crystal growth. Of course, if stoichiometric Si–C-based fibers were able to be fabricated, mechanical properties (stiffness, strength) would certainly be much improved, since the fiber would quickly become really polycrystalline and free of any intergranular phase with an increasing T_p. However, the peculiar texture of free carbon-containing Si–C-based ceramics is likely to ensure a flexibility which could be desirable for some applications. Finally, even though hydrogen is generally considered as a subordinate constituent because of its negligible weight contribution, its role appears very important regarding the behavior of free carbon and the subsequent evolution of the electrical properties. This study suggests that, by acting both on the carbon and the hydrogen contents of the starting material, both the moment of the semiconductor/conductor transition and the conductivity value could be controlled in materials from the Si–C system.

Acknowledgements

The authors wish to thank the National Program 'Précurseurs de céramiques à base Si, C, N, O' for its financial support and specifically the French National Research Council (CNRS), the French Ministry of Defence (DRET), Rhône-Poulenc and Société Européenne de Propulsion. They also thank C. Valhas for the thermodynamic advice, and A. Oberlin for helpful discussion.

References

1. Yajima, S., Hasegawa, Y., Hayashi, J. & Limura, M., Synthesis of continuous silicon carbide fiber. Part 1: Synthesis of polycarbosilane as precursor. *J. Mater. Sci.*, **13** (1978) 2569–76.
2. Hasegawa, Y., Limura, M. & Yajima, S., Synthesis of continuous silicon carbide fiber. Part 2: Conversion of polycarbosilane fibers into silicon carbide fibers. *J. Mater. Sci.*, **15** (1980) 720–8.
3. Yajima, S., Special heat-resisting materials from organometallic polymers. *Ceram. Bull.*, **6** (1983) 893–917.
4. Hasegawa, Y. & Okamura, K., Synthesis of continuous silicon carbide fiber. Part 3: Pyrolysis process of polycarbosilane and structure of the products. *J. Mater Sci.*, **18** (1983) 3633–48.
5. Hasegawa, Y. & Okamura, K., Synthesis of continuous silicon carbide fiber. Part 4: The structure of polycarbosilane as the precursor. *J. Mater. Sci.*, **18** (1983) 321–8.
6. Ichikawa, H., Machino, F., Mitsuno, S., Ishikawa, T., Okamura, K. & Hasegawa, Y., Synthesis of continuous silicon carbide fiber. Part 5: Factors affecting stability of polycarbosilane to oxidation. *J. Mater. Sci.*, **21** (1986) 4352–8.
7. Hasegawa, Y., Synthesis of continuous silicon carbide fiber. Part 6: Pyrolysis process of cured polycarbosilane fiber and structure of SiC fiber. *J. Mater. Sci.*, **24** (1989) 1177–90.
8. Taki, T., Okamura, K. & Sato, M., A study of the oxidation curing mechanism of polycarbosilane fibre by solid-state high resolution nuclear magnetic resonance. *J. Mater. Sci.*, **24** (1989) 1263–7.
9. Taki, T., Inui, M., Okamura, K. & Sato, M., Conversion process of polycarbosilane to SiC by solid-state high resolution NMR. *J. Mater. Sci. Lett.*, **8** (1989) 918–20.
10. Bouillon, E., Mocaer, D., Villeneuve, J. F., Pailler, R., Naslain, R., Monthioux, M., Oberlin, A., Guimon, C. & Pfister, G., Composition–microstructure–property relationships in ceramic monofilaments resulting from the pyrolysis of a polycarbosilane precursor at 800 to 1400°C. *J. Mater. Sci.*, **26** (1991) 1517–30.

11. Delverdier, O., Monthioux, M., Oberlin, A., Lavedrine, A., Bahloul, D. & Goursat, P., Thermal behaviour of polymer-derived ceramic. II. Si–C–N system from a new PVSZ precursor. *J. High Temp. Chem. Processes*, **1** (1993) 139–49.
12. Delverdier, O., Monthioux, M., Mocaer, D. & Pailler, R., Thermal behaviour of polymer-derived ceramic. III. Si–C–N system from a new PCSZ precursor. In *5th European Conference on Composite Materials Proceedings*, ed. A. R. Bunsell, J. F. Jamet & A. Massiah. Bordeaux, France, 1992, pp. 691–6.
13. Bouillon, E., Langlais, F., Pailler, R., Naslain, R., Cruège, F., Huong, P. V., Sartrou, J. C., Delpuech, A., Laffon, C., Lagarde, P., Monthioux, M. & Oberlin, A., Conversion mechanisms of a polycarbosilane precursor into an SiC-based ceramic material. *J. Mater. Sci.*, **26** (1991) 1333–45.
14. Yajima, S., Development of ceramics, especially silicon carbide fibres, from organosilicon polymers by heat treatment. *Phil. Trans. Royal Soc. London*, **A294** (1980) 419–26.
15. Pillot, J. P., Bacqué, E., Dunoguès, J. & Olry, P., Copolymérisation de dichlorosilanes avec des bischlorosilylmethanes, les produits obtenus et les utilisations des dits produits. French Patent 2599371, 1986.
16. Le Coustumer, P., Monthioux, M. & Oberlin, A., Thermal degradation mechanisms of a Nicalon fiber as deduced from TEM observations. In *International Symposium on Carbon Ext. Abstr.*, Tsukuba, Japan, Vol. I, 1990, pp. 182–5.
17. Le Coustumer, P., Monthioux, M. & Oberlin, A., Understanding Nicalon® fibre. *J. Eur. Ceram. Soc.*, **11** (1993) 95–103.
18. Oberlin, A. & Oberlin, M., Graphitizability of carbonaceous materials as studied by TEM and X-ray diffraction. *J. Microsc.*, **132** (1983) 353–63.
19. Oberlin, A., High resolution TEM studies of carbonization and graphitization. In *Chemistry and Physics of Carbon*, Vol. 22, ed. P. A. Thrower. Marcel Dekker, New York, 1989, pp. 1–143.
20. Monthioux, M., Oberlin, A. & Bouillon, E., Relationship between microtexture and electrical properties during heat-treatment of SiC fibre precursor. *Comp. Sci. Technol.*, **37** (1990) 21–35.
21. Le Coustumer, P., Monthioux, M. & Oberlin, A., Mécanismes de dégradation d'une fibre Nicalon série 200. In *Actes du Colloque AMAC–CODEMAC Matériaux Composites pour applications à hautes températures*, ed. R. Naslain, J. Lamalle & J. L. Zulian. Bordeaux, France, 1990, pp. 43–53.
22. Maire, J. & Méring, J., Graphitization of soft carbons. In *Chemistry and Physics of Carbon*, Vol. 6, ed. P. L. Walker. Marcel Dekker, New York, 1970, pp. 125–90.
23. Mah, T., Hecht, N. L., McCullum, D. E., Hoenigman, J. R., Kim, H. M., Katz, A. P. & Lipsitt, H. A., Thermal stability of SiC fibres (Nicalon®). *J. Mater. Sci.*, **19** (1984) 1191–201.
24. Laffon, C., Flank, A. M., Lagarde, P., Laridjani, M., Hagege, R., Olry, P., Cotteret, J., Dixmier, J. J., Miquel, L. Hommel, H. & Legrand, A. P., Study of Nicalon-based ceramic fibres and powders by EXAFS spectrometry, X-ray diffractometry and some additional methods. *J. Mater. Sci.*, **24** (1989) 1503–12.
25. Maniette, Y. & Oberlin, A., Interphase phenomena in silicon carbide single filament composites. *J. Mater. Sci.*, **25** (1990) 3864–74.
26. Le Coustumer, P., Etude du système Si–O–C: exemple de la fibre céramique Nicalon (série 200). PhD Thesis, University of Pau & Pays de l'Adour, France, 1991.
27. Bibbo, G. S., Benson, P. M. & Pantano, C. G., Effect of carbon monoxide partial pressure on the high-temperature decomposition of Nicalon fibre. *J. Mater. Sci.*, **26** (1991) 5075–80.
28. Maniette, Y. & Oberlin, A., TEM characterization of some crude or air heat-treated SiC Nicalon fibres. *J. Mater Sci.*, **24** (1989) 3361–70.
29. Delverdier, O., Evolution thermique de céramiques issues de polymères à base Si, C, N, O, H. PhD Thesis, University of Pau & Pays de l'Adour, France, 1991.